Analyzing flow characteristics and convective transport phenomenon of nanofluid flow inside a square cavity

Shahzad Munir, Yasar Amin, Rab Nawaz, Kishwat Ijaz Malik

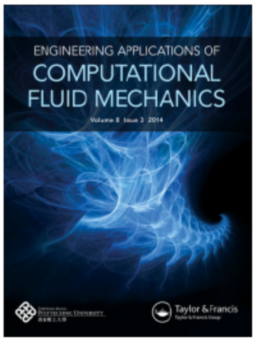

Engineering Applications of Computational Fluid Mechanics

ISSN: 1994-2060 (Print) 1997-003X (Online) Journal homepage: www.tandfonline.com/journals/tcfm20

Analyzing flow characteristics and convective transport phenomenon of nanofluid flow inside a square cavity

S. Munir, A. Amin, R. Nawaz & K. I. Malik

To cite this article: S. Munir, A. Amin, R. Nawaz & K. I. Malik (2025) Analyzing flow characteristics and convective transport phenomenon of nanofluid flow inside a square cavity, Engineering Applications of Computational Fluid Mechanics, 19:1, 2581730, DOI: 10.1080/19942060.2025.2581730

To link to this article: https://doi.org/10.1080/19942060.2025.2581730

Published online: 07 Nov 2025.

ENGINEERING APPLICATIONS OF COMPUTATIONAL FLUID MECHANICS
2025, VOL. 19, NO. 1, 2581730
https://doi.org/10.1080/19942060.2025.2581730

Analyzing flow characteristics and convective transport phenomenon of nanofluid flow inside a square cavity

S. Munir[a], A. Amin[a], R. Nawaz[b] and K. I. Malik[c]

[a]Department of Mathematics, COMSATS University Islamabad, Islamabad, Pakistan; [b]Centre for Applied Mathematics and Bioinformatics, Gulf University for Science and Technology, Mubarak Al-Abdullah, Kuwait; [c]Mechanical and Industrial Engineering, Montana State University, Bozeman, MT, United States

ABSTRACT

Efficient thermal management in confined spaces is a critical requirement in various fields, including biomedical applications like ureteroscopy, where precise temperature regulation is essential for patient safety and procedural efficacy. This study investigates the flow and heat transfer characteristics of copper-water nanofluids within a two-dimensional channel cavity, emphasizing the combined effects of convection and nanoparticle dynamics. Using the finite element method, the research systematically evaluates the influence of key parameters, including Reynolds number (Re), Grashof number (Gr), and nanoparticle volume fraction (ϕ), on thermal and flow behaviours. Quantitative analysis revealed that as Gr increased, isotherms aligned more horizontally due to enhanced buoyancy-driven convection, with a corresponding increase in the Nusselt number on heated walls by up to 85%. Conversely, an increase in ϕ reduced the Nusselt number by approximately 12%, highlighting the trade-off between nanoparticle-induced viscosity and thermal conductivity. The study also found that kinetic energy increased linearly with both Re and Gr, demonstrating intensified fluid motion and turbulence within the cavity. These findings are significant for optimizing fluid dynamics and thermal efficiency in medical procedures like ureteroscopy, where effective cooling and irrigation systems are critical. The insights into nanoparticle effects and convection mechanisms provide a foundation for designing energy-efficient and thermally optimized systems in biomedical devices and beyond. Future work should focus on experimental validation and exploring hybrid nanoparticle formulations to further enhance system performance.

ARTICLE HISTORY
Received 28 November 2024
Accepted 8 September 2025

KEYWORDS
Copper-water nanofluid; mixed convection; finite element method; cavity channel

Nomenclature

u, v	non-dimensional velocity components
Pr	Prandtl number
Re	Reynolds number
Gr	Grashof number
Re	Reynolds number
Nu	Nusselt number
Nu_{avg}	Average Nusselt number
β	thermal expansion coefficient
k	thermal conductivity
μ	dynamic viscosity
θ	temperatures (non-dimensional)
ϕ	volume fraction (non-dimensional)
T_c	temperature of cooled wall
T_h	temperature of heated wall
T_w	temperature of adiabatic wall
Cu	Copper nanoparticles
w	water
nf	nanofluid
f	water base fluid

1. Introduction

Kidney stones are solid mineral and salt deposits that form inside your kidneys. They can cause intense pain and discomfort as they pass through the urinary tract (Stamatelou et al., 2003; Scales et al.; Kum et al., 2016). Treatment options can vary depending on the size and location of the stones, as well as the severity of your symptoms. Ureteroscopy is a valuable medical procedure that plays a crucial role in the diagnosis and treatment of various conditions affecting the urinary tract, particularly the ureters and kidneys. It is commonly used for the removal of kidney stones. Small instruments can be passed through the ureteroscope to break up or remove stones lodged within the urinary tract. This minimally invasive approach reduces the need for open surgery and can help relieve the symptoms associated with kidney stones, such as pain and urinary obstruction. Ishii et al. (2015) illustrated a review for removal of stones in infants using ureteroscopy. Omar et al. (2015) explored the current trends in imaging methods

CONTACT K. I. Malik kishwatmalik@montana.edu Department of Mechanical and Industrial Engineering, Montana State University, PO Box 173860, Bozeman, MT 59717-3860, United States

used after ureteroscopy for stone removal. Wright et al. (2014) presented a detailed study on the present situation and upcoming anticipation of stone clearance procedure. Williams et al. (2020) illustrated the properties of fluid movement within an enclosed space and their practical uses in the context of extracting kidney stones. Moore et al. (2005) conducted a theoretical study on stone detection and their removal techniques.

Newtonian fluid dynamics is a branch of fluid mechanics that deals with the behaviour of fluids that follow Newton's law of viscosity. In Newtonian fluids, the rate of shear deformation is directly proportional to the applied shear stress. The importance and applications of Newtonian fluid dynamics are vast and encompass various fields of science, engineering, and everyday life. Blood, synovial fluid, and other bodily fluids often behave as Newtonian fluids under certain conditions. Medical procedures, drug delivery, and the functioning of medical devices require a grasp of how these fluids flow. A nanofluid is a suspension of nanoparticles in a base fluid, often water or oil. These nanoparticles are typically on the nanometer scale (1 to 100 nanometers) and are dispersed within the base fluid. The addition of nanoparticles to the fluid can lead to changes in its properties, such as thermal conductivity and viscosity. Choi (2009) presented a detailed review on nanofluid in his study. Munir and Amin (2024) explored a novel realm in nanofluid studies implementing nanofluids in two-layer channel flow. Yan et al. (2020) Utilized molecular dynamics simulations to examine the flow of Water-Copper nanofluid within a three-dimensional nanochannel, considering various surface roughness geometries, aimed at enhancing energy efficiency management. Influence of particle morphology and radiation impact on the Marangoni boundary layer flow and thermal characteristics of a copper-water nanofluid propelled by changing temperature was demonstrated by Lin et al. (2016). Wang et al. (2013) studied thermal exchange mechanism in a compact loop heat pipe using a water-copper nanofluid and found that copper nanofluid has better thermal conductivity than ordinary fluid. Ganesan et al. (2018) presented an experimental study on the use of copper-water nanofluid for small scale greasing in the bending process of steel.

The finite element method (FEM) is a numerical technique used for solving a wide range of engineering and scientific problems that involve partial differential equations (PDEs). It's particularly well-suited for problems where the geometry is complex or irregular, and analytical solutions are difficult to obtain. The basic idea behind FEM is to divide a complex problem domain into smaller, simpler subdomains called 'finite elements'. Many scientists have utilized FEM in finding their results on Newtonian and non-Newtonian fluid dynamics. Eid et al. (2022) utilized finite element approach to analyze the magnetohydrodynamic flow of a viscous fluid caused by a porous surface. Ali et al. (2021) investigated the effects of magnetism on thermal exchange characteristics in a lid-driven cavity filled with non-Newtonian fluid in the presence of an object. Bilal et al. (2021) studied conducting finite element calculations to manage non-Newtonian fluid dynamics within a space containing a cold round cylinder. Influence of a heat-conducting horizontal square block on mixed convection within a square cavity with ventilation using finite element method was explored by Rahman et al. (2009). References (Ahmad et al., 2024; Dutta et al., 2021; Gao et al., 2019; Malik et al., 2024; Munir & Turabi, 2024; Nguyen & Sagar, 2024; Turabi & Munir, 2024) provide further insight on different numerical schemes including FEM for similar problems.

Mixed convection holds significant importance in fluid dynamics due to its frequent occurrence in both natural and engineered systems. It involves the combined effects of buoyancy-driven flows and externally induced forces, which govern the transport of heat and momentum. This phenomenon serves as a link between pure natural convection and forced convection, enabling a more comprehensive analysis of fluid behaviour in real-world scenarios. Amin et al. (2024) explored the convective transport of Casson hybrid nanofluid in a two layered vertical channel. Ahmad et al. (2024) presented an investigation of mixed convective flow inside a cavity with porosity effects and found that the Nusselt number increases with thermal conductivity but decreases on increasing porosity. Lu et al. (2018) studied a computational analysis of a Newtonian fluid in a three-layer channel with convection effects using OHAM. Basak et al. (2009) investigated a mixed convection analysis in a channel with equal sides.

As research elucidated earlier, numerous researchers have dedicated their efforts to investigating the intricacies of flow dynamics within cavities using finite element method this study delves into the intricate dynamics of copper nanofluid flow within a channel cavity. This unique cavity structure is characterized by two walls, both of which are maintained at elevated temperatures. Unlike conventional fluids, nanofluids offer enhanced thermal properties, yet their behaviour within the geometric constraints of a square cavity remains underexplored. The research focuses on the effects of nanoparticle parameters (type, size, and volume fraction) and governing factors (e.g. Rayleigh number) on flow and heat transfer. The novelty lies in optimizing convective transport, understanding non-linear interactions, and minimizing entropy generation, with applications in microelectronics cooling, solar energy systems, and biomedical devices.

The study of nanofluid flow in a square cavity is innovative due to its focus on enhancing heat transfer through advanced nanofluid properties under confined conditions. It explores the interplay of nanoparticle characteristics, cavity geometry, and thermal parameters, addressing gaps in understanding non-linear flow dynamics and entropy generation. Scientifically, it provides insights into optimizing thermal performance, with applications in energy-efficient systems like microelectronics cooling, solar collectors, and biomedical devices, advancing both fluid dynamics research and practical thermal management solutions. Recent research has focused on the behaviour of nanofluids in a variety of applications, with major advances in understanding their flow and heat transmission properties. Zhou et al. (2024) investigate the cavitation performance of ice-blocked propellers, emphasizing the importance of surface effects on fluid dynamics, which can also be used to understand the behaviour of nanofluids in confined areas. Zhang et al. (2025) investigate the impacts of soft magnetic particles in composite materials, yielding important insights into the interactions of magnetic fields with nanofluid dynamics in complex flow channels. Furthermore, Z. Li et al. (2024) look into the performance optimization of magnetic fluid seals, providing a framework for understanding the multi-physics behaviour of nanofluids under different conditions. Zeng et al. (2024) diagnose multi-cavitation states in vortex pumps, which is significant for the development of nanofluid-based thermal systems. D. Li and Li (2024) investigate electromagnetohydrodynamic (EMHD) flow in microchannels, which is important for understanding the behaviour of nanofluids in constrained spaces. Sun et al. (2024) investigate shear thickening fluids experimentally, providing insights into nanofluid dynamics that can be applied to damping systems in thermal management applications. Han et al. (2018) investigate superlubricity and its potential impact on nanofluid behaviour. Sarmiento-Laurel et al. (2022) provide a model for entropy formation in fluid flows, which could help improve the efficiency of nanofluid thermal management systems. Zandie et al. (2022) investigate the effect of magnetic fields and nanoparticles on phase transition materials, which has direct implications for increasing nanofluid thermal conductivity. Finally, Mahdavi et al. (2020) report a simulated analysis of nanofluid flow between parallel plates, which adds to our understanding of shear layers and heat transfer mechanisms. These research collectively improve our understanding of nanofluid behaviour and its prospective applications in a variety of sectors, including energy-efficient systems, microelectronics cooling, and biomedical devices. Thus, a noteworthy application of this research lies within the field of ureteroscopy, a medical procedure involving the exploration of the urinary tract using specialized instruments. Enhanced knowledge of fluid behaviour and temperature distribution can aid in optimizing the design of instruments, improving visualization during procedures, and ensuring patient comfort and safety.

We acknowledge that this study has various limitations that may affect the interpretation of our findings. Firstly, as a theoretical analysis based on FEM simulations, the work lacks experimental validation, which could lead to inconsistencies with real-world behaviour. Idealized assumptions, such as uniform nanoparticle dispersion and constant thermophysical characteristics, may not adequately reflect real-world settings where particle agglomeration and non-homogeneous distributions might influence flow dynamics. Furthermore, our study focuses solely on steady-state settings and does not investigate transient behaviours, which may be crucial in time-dependent systems. The study also excludes extrinsic effects like as temperature changes, pressure gradients, and non-Newtonian fluid behaviour, all of which could have an impact on real-world applications. Furthermore, while we investigated the effects of Reynolds number, Grashof number, and nanoparticle volume fraction, we did not address factors such as particle size, shape, concentration distribution, or the potential impact of hybrid nanoparticles. Future work could address these limitations by incorporating experimental validation, transient flow analysis, and other relevant parameters.

2. Flow model and geometry

The research focuses on investigating the intriguing behaviour of water-copper-based nanofluids within a square cavity channel configuration. This channel with a length $L = 1$, serves as a controlled environment to study the fluid dynamics and heat transfer phenomena occurring within it. To create distinct thermal gradients, hot and cold temperatures are applied to the channel's right and left walls respectively. The left wall have temperature T_h, the right wall have T_c and the remaining walls (denoted as Γ_{wall}) are adiabatic. The nanofluid, composed of water and copper nanoparticles, is introduced through the inlet located at $\{(x, y); x = 0, y\epsilon[0.4, 0.6]\}$. It exits the channel through two outlets defined as $\{(x, y); x = 0, y\epsilon[0, 0.15] \cup [0.85, 1]\}$.

The physical model of the problem is illustrated in Figure 1, and the thermophysical properties of the nanofluid and base fluid can be found in Tables 1 and 2, respectively.

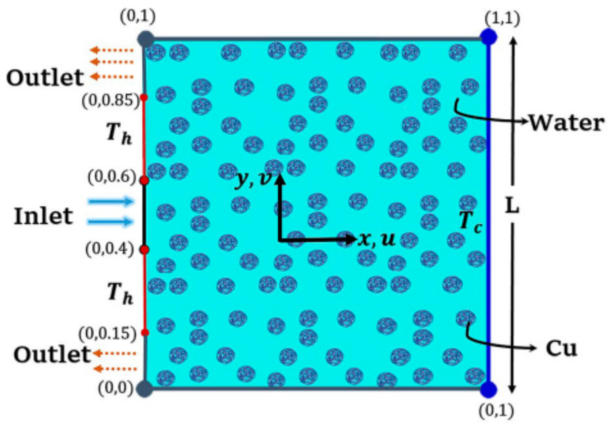

Figure 1. Schematic diagram of the cavity flow.

Table 1. Thermophysical properties of nanofluid (Dutta et al., 2021).

Characteristics	Nanofluid ($Cu - water$)
μ (viscosity)	$\frac{\mu_{nf}}{\mu_f} = (1-\phi_{Cu})^{-2.5}$
ρ (density)	$\frac{\rho_{nf}}{\rho_f} = \left((1-\phi_{Cu}) + \phi_{Cu}\frac{\rho_{Cu}}{\rho_f}\right)$
ρc_p (heat capacity)	$\frac{(\rho c_p)_{nf}}{(\rho c_p)_f} = \left((1-\phi_{Cu}) + \phi_{Cu}\frac{(\rho c_p)_{Cu}}{(\rho c_p)_f}\right)$
k (Thermal conductivity)	$\frac{k_{nf}}{k_f} = \frac{k_{Cu}+2k_f-2\phi_{Cu}(k_f-k_{Cu})}{k_{Cu}+2k_f+\phi_{Cu}(k_f-k_{Cu})}$
β(Thermal expansion coefficient)	$\frac{(\rho\beta)_{nf}}{(\rho\beta)_f} = \left((1-\phi_{Cu}) + \phi_{Cu}\frac{(\rho\beta)_{Cu}}{(\rho\beta)_f}\right)$

Table 2. Thermophysical properties of copper nanoparticles and water (Dutta et al., 2021).

Properties	Water	Copper
k	0.613	401
ρ	997.1	8954
β	2.1×10^{-4}	1.67×10^{-5}
c_p	4179	383
μ	8.91×10^{-5}	–

Following assumptions are considered for the underlying flow problem:

- The flow is modelled as two-dimensional and steady-state, ensuring a simplified yet representative analysis of the problem.
- The fluid is assumed to be incompressible, allowing the neglect of density variations due to pressure changes.
- The cavity channel under consideration has a non-dimensionalized length $L = 1$, providing a standardized framework for comparative studies.
- The density and specific heat capacity of the nanofluid are assumed to remain constant, simplifying the mathematical modelling while maintaining physical relevance.
- The thermophysical properties of the nanofluid, such as thermal conductivity and viscosity, are computed based on Maxwell's effective medium theory, ensuring accurate representation of the nanofluid behaviour.
- Differential heating is applied, with the channel's right wall maintained at a hot temperature and the left wall at a cold temperature, creating a thermal gradient driving the flow.

The dimensionless continuity, momentum and energy equations (Ali et al., 2021) are:

$$\frac{\partial u}{\partial x} + \frac{\partial v}{\partial y} = 0, \tag{1}$$

$$u\frac{\partial u}{\partial x} + v\frac{\partial u}{\partial y} = -\frac{\partial p}{\partial x} + \frac{A}{Re}\left(\frac{\partial^2 u}{\partial x^2} + \frac{\partial^2 u}{\partial y^2}\right), \tag{2}$$

$$u\frac{\partial v}{\partial x} + v\frac{\partial v}{\partial y} = -\frac{\partial p}{\partial x} + \frac{A}{Re}\left(\frac{\partial^2 v}{\partial x^2} + \frac{\partial^2 v}{\partial y^2}\right) + B\frac{Gr}{Re^2}\theta, \tag{3}$$

$$u\frac{\partial \theta}{\partial x} + v\frac{\partial \theta}{\partial y} = \frac{C}{Re\,Pr}\left(\frac{\partial^2 \theta}{\partial x^2} + \frac{\partial^2 \theta}{\partial y^2}\right), \tag{4}$$

where Pr, Re, Gr defines the Prandtl number, Reynolds number, Grashof number, respectively. u be the velocity in x direction and v be the velocity in y direction, θbe the temperature, p be the pressure. Equation (1) represents the Continuity equation for the incompressible fluid (White & Majdalani, 2006) which implies that the divergence of velocity is zero, meaning the volume of fluid entering a control volume equals the volume leaving it. Equations (2)–(3) are two-dimensional momentum equations in x and y directions (White & Majdalani, 2006) commonly encountered in fluid dynamics. These include terms for inertial effects, pressure gradients, viscous diffusion, and buoyancy-driven force. Left side of these equations represent the convective acceleration which represent changes in the velocity component due to motion of the fluid in x and y directions respectively. $\frac{\partial p}{\partial x}$ and $\frac{\partial p}{\partial y}$ represent the force driving fluid motion in x and y direction caused by a pressure difference respectively. Second term in Equations (2) and (3) defines the viscous diffusion. It represents viscous effects that resist motion and smooth out velocity gradients in $x$and $y$directions respectively.Redenotes Reynolds number. $\frac{Gr}{Re^2}\theta$denotes the buoyancy term which accounts for buoyancy effects due to temperature variations in the fluid. Gr be the Grashof number and θ be the dimensionless temperature field. Equation (4) is the energy equation (White & Majdalani, 2006) of two dimensional flow which describes the transport of dimensionless temperature field. In this equation, terms on left side represents convective heat transfer. This term shows how the temperature field changes as fluid particles move in the x

and y direction. Term on the right side denotes the diffusive heat transfer which represents the heat conduction within the fluid. Pr be the Prandtl number, a dimensionless number that is ratio of momentum diffusivity to thermal diffusivity.

The boundary conditions associated with the governing problem are as follows (Williams et al., 2020):

$$u = 1 - y^2,\ v = 0\ on\ \Gamma_{in}, \tag{5}$$

$$2\frac{\partial u}{\partial x} - P = 0,\ \frac{\partial u}{\partial y} + \frac{\partial v}{\partial x} = 0\ on\ \Gamma_{out} \tag{6}$$

$$u = v = 0\ on\ \Gamma_{wall} \tag{7}$$

$$\theta = 0\ on\ T_c \tag{8}$$

$$\theta = 1\ on\ T_h. \tag{9}$$

having dimensionless boundaries defined as

$$\Gamma_{in} = \{(x,y); x = 0, y\epsilon[0.4, 0.6]\} \tag{10}$$

$$\Gamma_{out} = \{(x,y); x = 0, y\epsilon[0, 0.15] \cup [0.85, 1]\} \tag{11}$$

$$\text{cool wall} = \{(x,y); x = 1, y\epsilon[0, 1]\} \tag{12}$$

$$\text{heated wall} = \{(x,y); x = 0, y\epsilon[0.15, 0.4] \cup [0.6, 0.85]\} \tag{13}$$

$$\Gamma_{wall} = \Gamma\ \backslash\{\Gamma_{in} \cup \Gamma_{out}\} \tag{14}$$

$$A = (1-\phi)^{-2.5}, C = \frac{k_{nf}}{k_f}, B = \frac{(\rho\beta)_{nf}}{(\rho\beta)_f}$$

$$Pr = \frac{\vartheta}{\alpha}, Re = \frac{UL}{\vartheta}, Gr = \frac{g\beta(T_h - T_c)L^3}{\vartheta^2}$$

2.1. Grid convergence analysis

To assess the effectiveness of the present results, a broad range of grids is employed under specific conditions with parameters such as$Gr = 10^3, Pr = 6.8, Re =$ 1and$\phi = 0.01$. These grids are detailed in Table 3, with varying degrees of freedom (DOFs) spanning from 532 to 36152 and total number of elements (NEL) ranging from 180 to 16441. Notably, the average Nusselt numbers exhibit negligible differences for the last two grids (Grids 7 and 8). Consequently, a grid with DOFs of 14556and NEL of 6435 ensures grid independence, and the numerical results are reported based on these specific DOFs and NEL values.

2.2. Average Nusselt number and kinetic energy

The average Nusselt number is determined by calculating the average of local Nusselt numbers across the overall thermal exchange surface, and its magnitude is influenced by the specific geometry or surface properties involved in the heat transfer process. The average Nusselt can be computed from the following expression (Dutta et al., 2021):

$$Nu_{avg} = \int_0^1 Nu dY$$

where Nu denotes the local Nusselt number as

$$Nu = -\frac{k_{nf}}{k_f}\frac{\partial\theta}{\partial X}.$$

In addition to the parameters above, it is interesting to calculate and examine a quantity known as the total kinetic energy, defined as:

$$Kinetic\ energy = \frac{1}{2}\int_{\Omega}^{1} U^2 d\Omega$$

Where U is the velocity vector (u, v).

Table 3. Grid convergence analysis for average Nusselt number (upper and lower wall) and kinetic energy (K.E).

Grid	NEL	DOFs	Nu_{avg} (Upper wall)	Nu_{avg} (Lower wall)	K.E
1	180	532	1.4721	2.6796	1.1184
2	334	928	1.5710	2.7819	1.1518
3	534	1396	1.6737	2.8855	1.1546
4	963	2428	1.8297	3.0290	1.1564
5	1466	3560	1.9378	3.1274	1.1585
6	2442	5668	2.0150	3.2097	1.1696
7	6435	14556	2.2323	3.4579	1.1749
8	16441	36152	2.3781	3.6292	1.1764

3. Results and discussions

To study the current problem of nanofluid flow and heat transfer, we have taken a square channel and set distinct hot and cold temperatures on the right and left walls respectively. FEM based COMSOL Multiphysics is utilized to simulate the flow with the non-dimensional governing equations. It is a versatile software platform that is indeed commonly used for observing and simulating flow dynamics and heat transfer in various engineering and scientific applications. It provides a powerful environment for setting up and solving complex problems, including fluid flow and heat transfer simulations. Velocity streamlines and isotherm patterns are plotted to visualize variations in distributions.

3.1. Velocity streamlines

Figure 2(a–f) illustrates the happenings in velocity streamlines for different Reynolds numbers (Re). This study deals with Reynolds number ranges from 1 to 1000.

At low Reynolds numbers, the flow moves with minimal mixing and one clockwise rotating eddy is observed in the centre of the channel. This eddy is weak and hardly made an impact on flow dynamics due to low kinetic energy as given in Table 5. For $Re = 50$ and 100, two counter rotating structures of same magnitude are observed near the inlets which later grew in size. These vortices stirred the fluid, and a large amount of surrounding fluid is trapped by the engulfing surface. Lately, these vortices transported molecular fluid into the mean flow. This mechanism eventually enhances system efficiency by improved mixing. The total circulation of this domain is equal to zero because each vortex, although it has the same magnitude, is operating in opposite directions. Moreover, due to no slip conditions at the channel walls, the vortices developed more shear ahead than below. For $Re = 500$ and 1000, the vortex in the upper region of the channel gained momentum from the mean flow and moved in the lateral direction. This vortex developed recirculation zones and suppressed the vortex beneath it. The presence and size of these recirculation zones and vortices depend on the Reynolds number.

The crucial finding from this discussion states that as the Reynolds number increases, flow dynamics evolve significantly, with counter-rotating vortices enhancing mixing at moderate Re (50–100) and the formation of dominant recirculation zones at high Re (500–1000). These recirculation zones are crucial as they improve mixing efficiency and highlight the strong dependence of flow behaviour on Reynolds number.

Figure 3(a–d) shows the effect of Grashof number on velocity streamlines. The Grashof number is a dimensionless parameter that represents the ratio of buoyancy forces to viscous forces in a fluid flow due to temperature differences. It is often used to predict the onset of natural convection, which is the flow of fluid induced solely by temperature gradients. In the context of a channel cavity with heated walls and the insertion of a copper nanofluid, the Grashof number will influence the formation of vortices and the behaviour of streamlines due to natural convection. The Grashof number directly affects the size and intensity of the vortices. In a channel cavity with heated walls, higher Grashof numbers will lead to the development of larger and more energetic vortices. For higher values of Grashof number, the dominance of buoyancy forces squeezes the vortex near the centre of the cavity and due to this another small vortex is formed at the other end. These vortices can influence the mixing of the copper nanofluid and the distribution of temperature within the fluid. Summing up, higher Grashof numbers intensify buoyancy forces, leading to larger and more energetic vortices in the cavity. This results in enhanced mixing and temperature distribution within the copper nanofluid. At higher Grashof values, a dominant vortex near the cavity centre compresses, forming a secondary smaller vortex, further influencing fluid behaviour and heat transfer.

3.2. Results of isotherms

Figure 4(a–d) presents the influence of Reynolds number on isotherms. As the Reynolds number rises, the isotherms become vertical and parallel. This is because in laminar flow, isotherms tend to be more gently curved following the orderly flow patterns. The temperature distribution in laminar flow is more influenced by conduction within the fluid and the development of thermal boundary layers. As the Reynolds number increases in laminar flow, the behaviour of isotherms may become slightly more curved or distorted, but they still exhibit a relatively ordered pattern compared to the more chaotic behaviour observed in turbulent flow. It is also evident that for higher values of Reynolds number, the temperature tends to spread to the far end of the cavity which was initially near the inlet zones for small Reynolds number. Briefly speaking, the Reynolds number increases, isotherms transition from curved to vertical and parallel, indicating enhanced convection and reduced conduction dominance. Higher Reynolds numbers also cause the temperature distribution to extend further into the cavity, moving away from the inlet zones observed at lower Reynolds values. This reflects the increased thermal transport efficiency with rising Reynolds numbers.

Figure 5(a–d) reveals the effect of Grashof number on isotherms. On increasing Grashof number, the isotherms become horizontal and parallel. The Grashoff number is a dimensionless parameter that quantifies the relative strength of buoyancy forces to viscous forces in a fluid flow and heat transfer process. When the Grashof number is sufficiently high, the buoyancy-induced fluid motion causes the formation of well-defined, horizontal isotherms. These isotherms indicate that the temperature gradient across the fluid is primarily in the vertical direction, with minimal temperature variation in the horizontal direction. Thus, as the Grashof number increases, isotherms become horizontal and parallel, indicating a dominance of buoyancy forces over viscous forces. This pattern reflects a vertical temperature gradient with minimal horizontal variation, characteristic of buoyancy-driven convection in high Grashof number flows.

Figure 6(a–d) shows the effect of nanoparticles volume fraction (ϕ) on isotherms. Nanoparticles typically have higher thermal conductivity than base fluid. As we increase ϕ, the overall thermal conductivity of

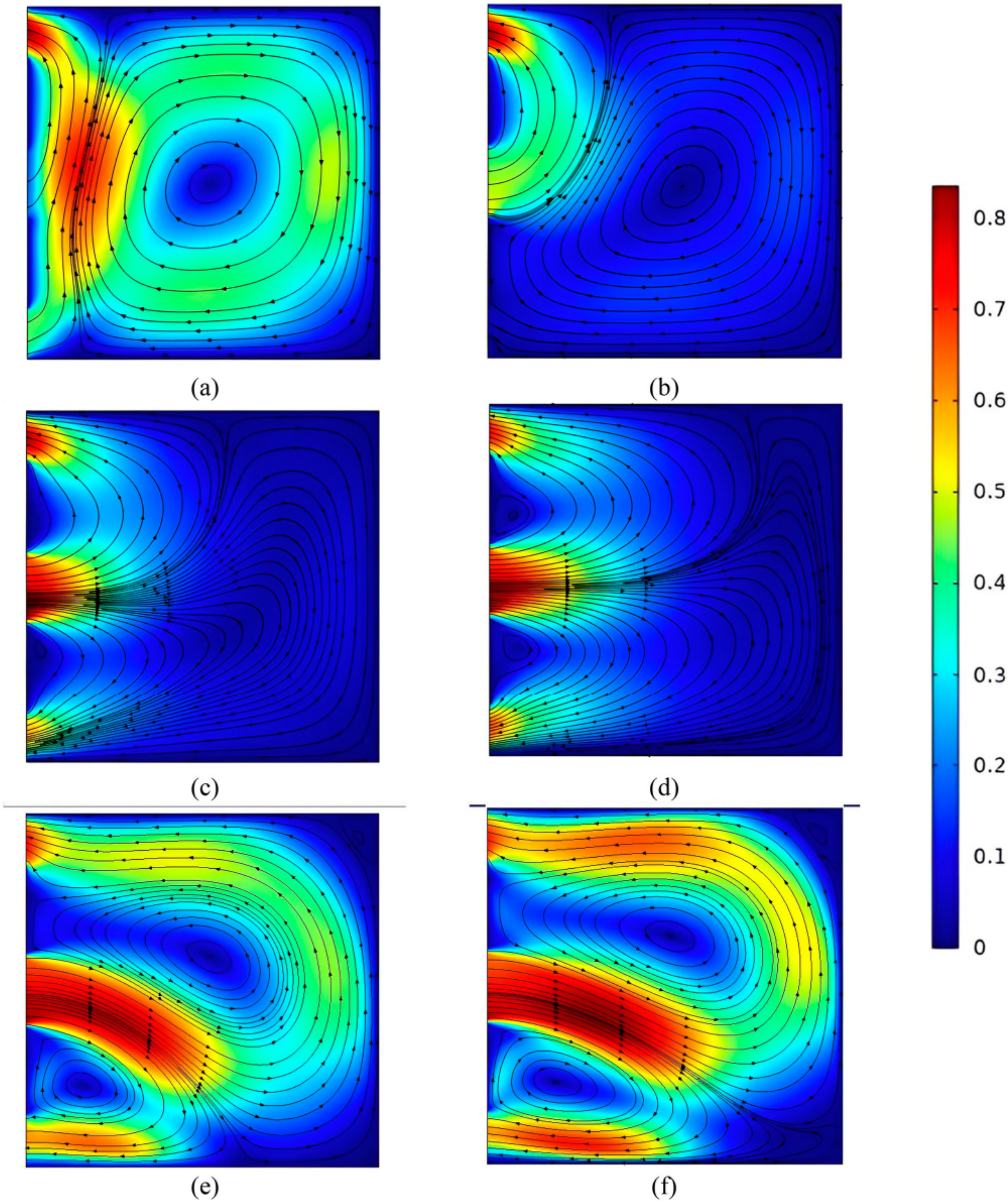

Figure 2. (a–f) Streamlines variation for $Re = 1, 10, 50, 100, 500, 1000$.

the nanofluid increases. Higher thermal conductivity means that heat is conducted more effectively within the fluid. This can lead to flatter isotherms, especially near the heated surface, as heat spreads more evenly through the nanofluid. Eventually, as the nanoparticle volume fraction increases, the thermal conductivity of the nanofluid improves, leading to more efficient heat conduction. This results in flatter isotherms, particularly near the heated surface, as heat spreads more uniformly through the nanofluid.

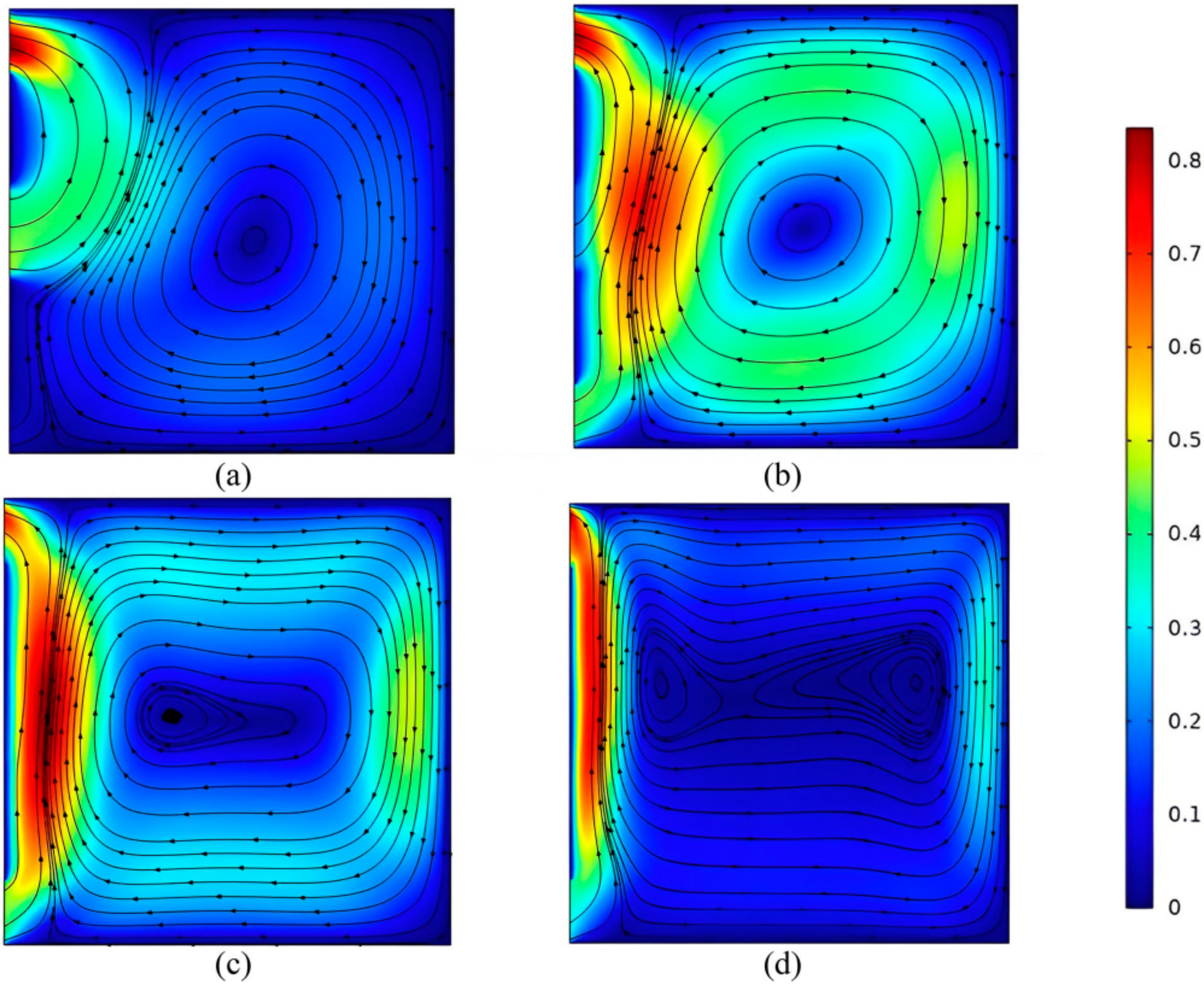

Figure 3. (a–d) Streamline variations for $Gr = 10^2, 10^3, 10^4, 10^5$.

Table 4 shows as expected the decreasing behaviour of average Nusselt number for both walls on increasing Reynolds number and Grashof number. Nu_{avg} for upper and lower walls decreases on increasing Re while opposite behaviour has seen in case of Gr for both walls. Table 5 presents the variation of kinetic energy on increasingRe and Gr. This is because at low Reynolds numbers, the flow is often laminar, characterized by smooth and ordered fluid motion. As the Reynolds number increases, the flow is more likely to transition from laminar to turbulent. Turbulent flow involves complex, chaotic, and irregular fluid motion with various eddies and vortices forming in the fluid. These eddies and vortices contribute to a greater kinetic energy content in the fluid.

Higher Grashof numbers indicate stronger buoyancy forces relative to viscous forces. This leads to more significant fluid movement due to natural convection. As fluid parcels experience density variations due to temperature differences, they become buoyant, leading to fluid motion characterized by vortices and circulation cells. Hence, kinetic energy increases.

Table 4. Values of average Nusselt number (upper and lower wall) on varying Reynolds number and Grashof number.

Re	Gr	Nu_{avg} (Upper wall)	Nu_{avg} (Lower wall)
1		2.3941	3.6337
10		0.47373	3.4180
50		3.5493×10^{-4}	0.18345
100		2.3165×10^{-4}	0.00796
	10^2	1.5474	1.7831
	10^3	2.3741	3.6337
	10^4	5.6456	8.5979
	10^5	13.766	19.880

Figure 7(a–b) explores the influence of Gr on Nusselt number for both upper and lower heated walls. Higher Grashof numbers result in more vigorous fluid movement, which enhances heat transfer through increased fluid mixing and contact with heated walls. This can lead

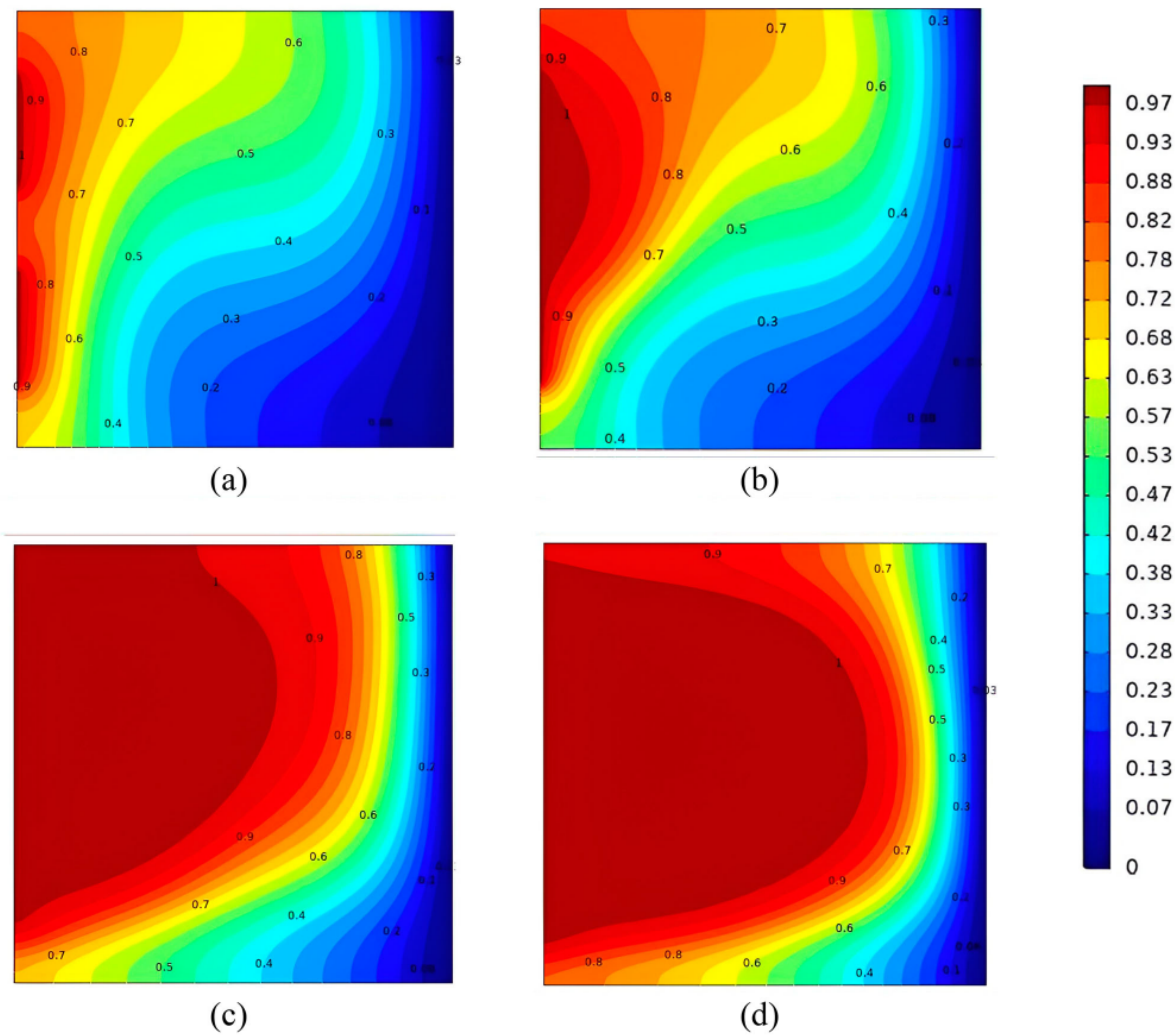

Figure 4. (a–d) Isotherm distribution for $Re = 1, 10, 50, 100$.

Table 5. Influence of Reynolds number and Grashoff number on Kinetic energy.

Re	*Gr*	Kinetic energy
1		1.1764
10		2.01972
50		4.02324
100		7.03751
	10^2	0.056111
	10^3	1.17490
	10^4	10.1980
	10^5	54.4631

to a higher Nusselt number on both heated walls, indicating improved convective heat transfer compared to conductive heat transfer.

Figure 8(a–b) shows the decreasing behaviour of Nusselt number for upper and lower heated wall on increasing volume fraction of nanoparticles. The addition of nanoparticles can also alter the viscosity of the fluid. An increase in viscosity can hinder fluid flow, reducing the convective heat transfer. As *Nu* is dependent on convective heat transfer, this can lead to a decrease in *Nu*. In fact, increasing the volume fraction of nanoparticles in a base fluid raises its viscosity, affecting flow behaviour dramatically. Higher viscosity lowers the mobility of fluid particles, resulting in a slower flow. This, in turn, reduces the efficiency of convective heat transmission since fluid mobility is essential for thermal energy transfer. Furthermore, greater viscosity can prevent the production of turbulent eddies, which are required for effective heat mixing in convective processes. As a result, the heat dissipation capability drops, which is reflected in the lower Nusselt number.

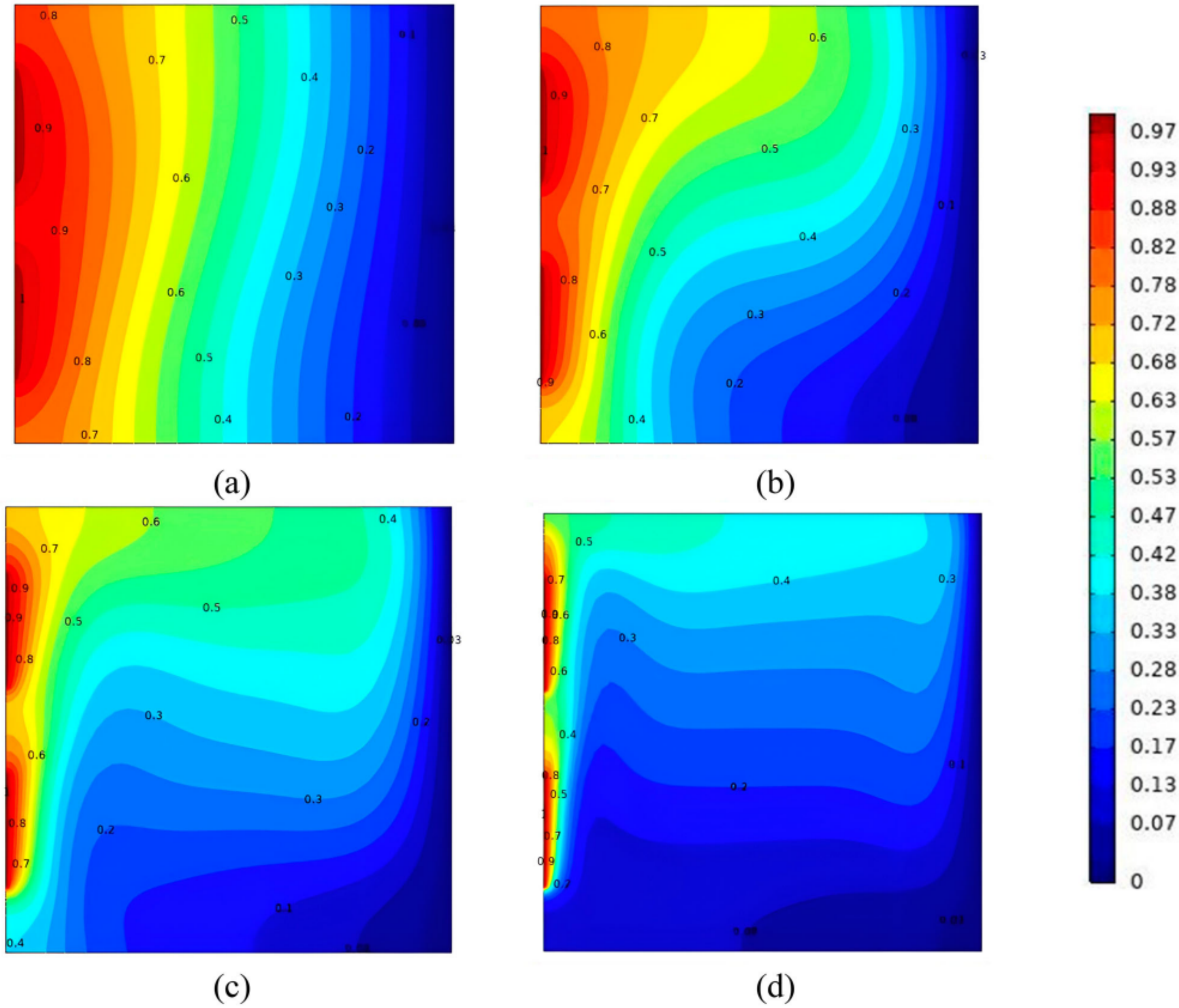

Figure 5. (a–d) Isotherm distribution for $Gr = 10^2, 10^3, 10^4, 10^5$.

4. Comparison of results

After doing a grid convergence analysis, we compared the computational results with the laminar flow available in Williams et al. (2020). Figure 9(a–b) shows velocity streamlines fixed at $Re = 34$ for existing and present results respectively. It is evident that present numerical results align well with the calculations based on the correlation.

5. Conclusions

In this study, we employed FEM to investigate the impact of convection on the flow of a nanofluid, consisting of a Newtonian fluid and nanoparticles, within a channel cavity. Through our analysis, we explored the effects of key parameters including Reynolds number, Grashof number, and volume fraction of nanoparticles. The key conclusions drawn from our investigation are as follows:

- As the Grashof number (Gr) increases, indicating a stronger influence of buoyancy forces relative to viscous forces, we observed a notable alteration in the isotherm patterns. Specifically, the isotherms became more horizontally oriented and parallel to each other. This behaviour is attributed to the intensified convective heat transfer within the cavity.
- With an increase in Reynolds number (Re), representing the ratio of inertial forces to viscous forces, the isotherms exhibited a vertical and parallel pattern. This phenomenon indicates enhanced fluid mixing and convective heat transfer within the channel, leading to more efficient heat dissipation.

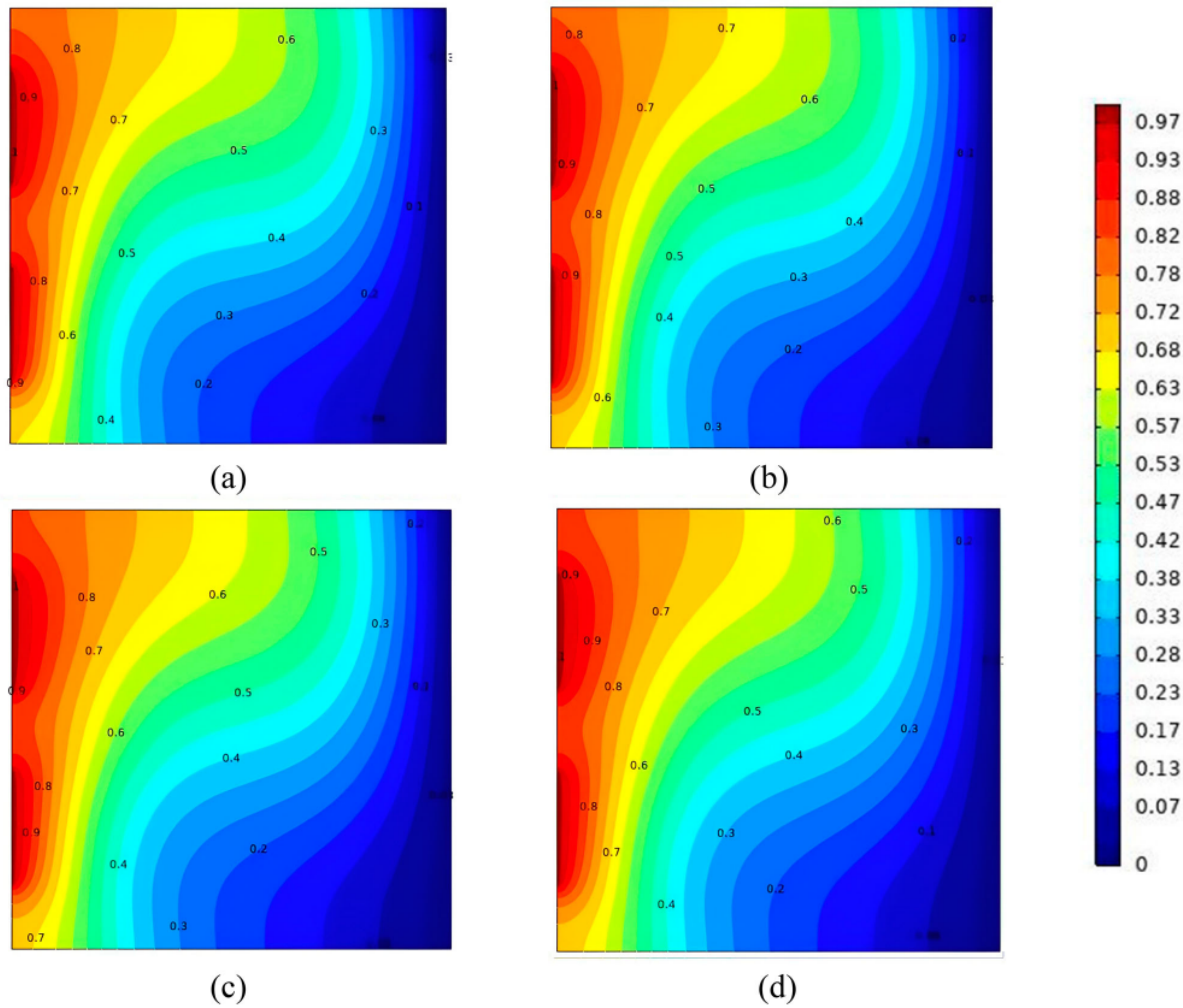

Figure 6. (a-d) Isotherm distribution for $\phi = 0.01, 0.03, 0.05, 0.07$.

- The Nusselt number, which characterizes the convective heat transfer coefficient, demonstrated a significant increase for both heated walls as the Grashof number was elevated. This trend reflects the heightened convective heat transfer resulting from the intensified fluid motion induced by buoyancy forces.
- Conversely, an increase in the volume fraction of nanoparticles led to a decrease in the Nusselt number for both heated walls. This observation suggests that the presence of nanoparticles hinders convective heat transfer within the nanofluid, possibly due to increased viscosity and reduced thermal conductivity.
- The kinetic energy for both walls exhibited a consistent increase with increasing values of Reynolds number and Grashof number. This behaviour indicates enhanced fluid motion and turbulence within the cavity, contributing to more efficient heat transfer.
- Furthermore, the average Nusselt number exhibited a decline with rising values of the volume fraction of nanoparticles. This trend underscores the negative impact of nanoparticle addition on convective heat transfer efficiency within the nanofluid.

The conclusions of this theoretical study gave a framework for practical applications, such as ureteroscopy. While this study does not include experimental validation or direct evidence from ureteroscopy, it does provide a foundation by examining the effects of important parameters like Reynolds number, Grashof number, and nanoparticle volume fraction on nanofluid dynamics. These characteristics have a significant impact on flow behaviour and heat dissipation, which is vital for building effective thermal management systems in medical equipment. Specifically:

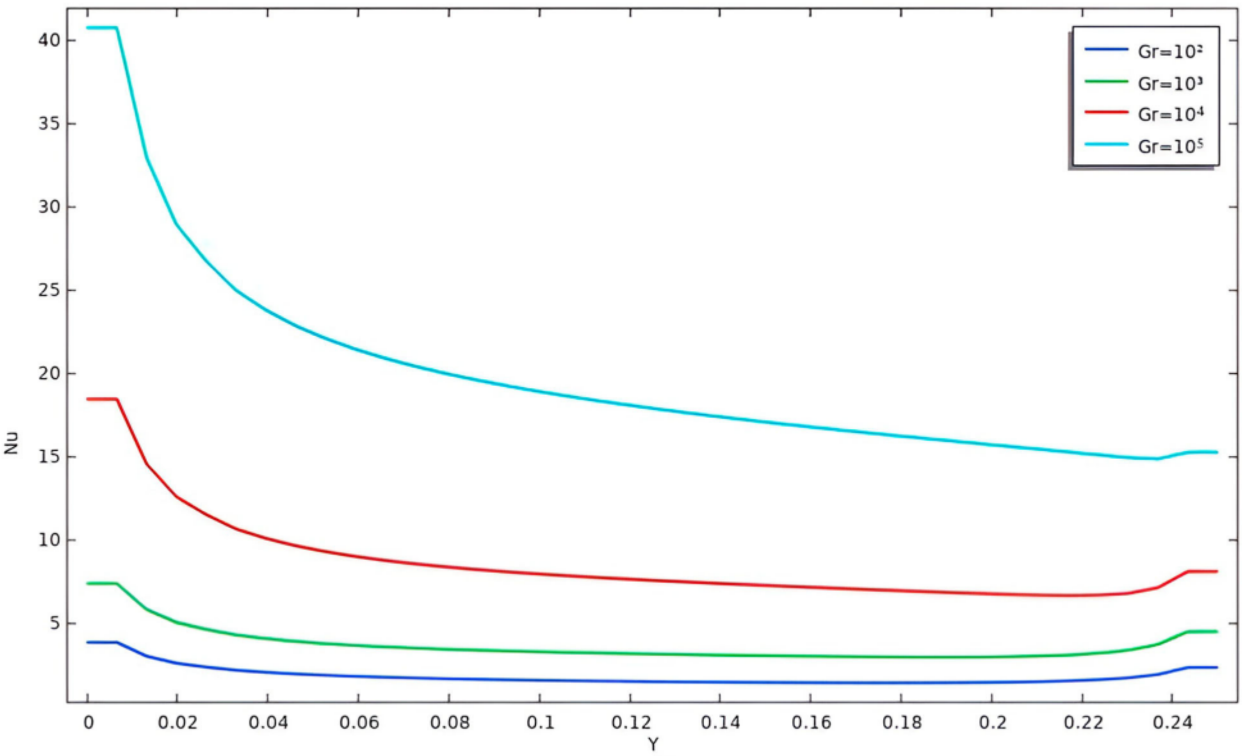

(a)

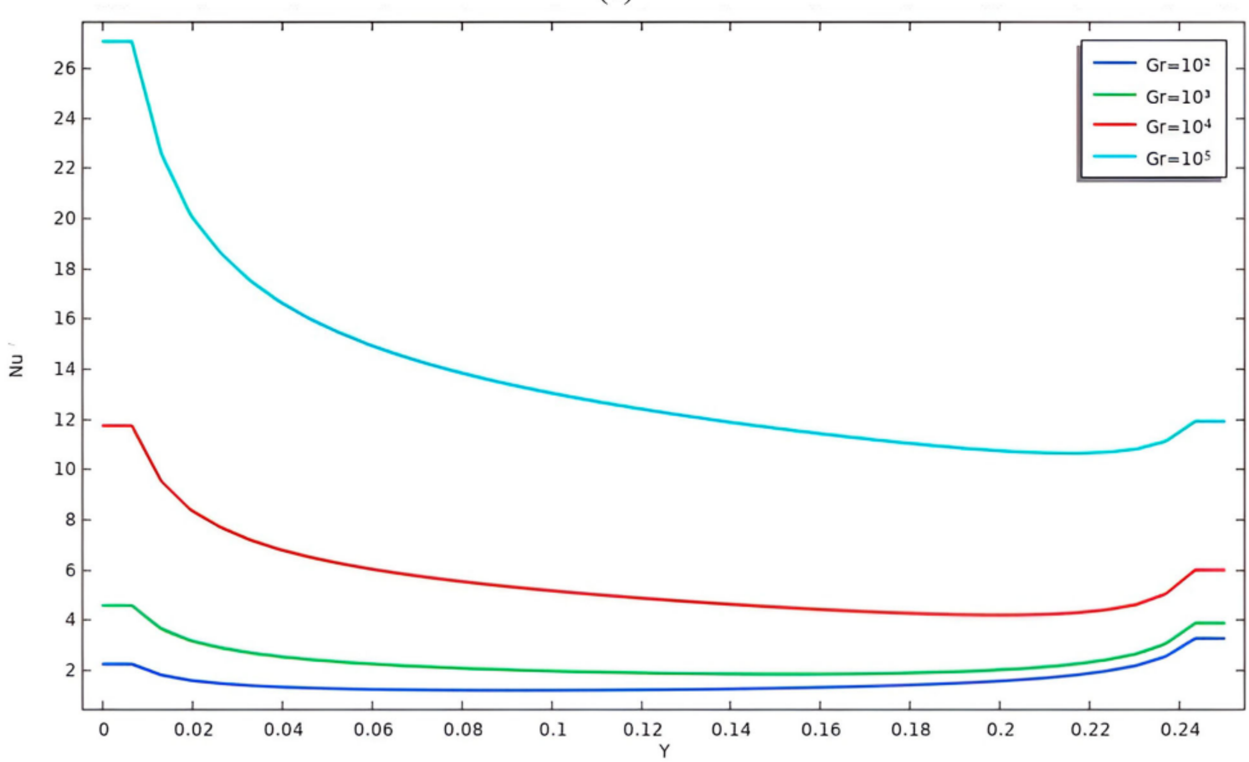

(b)

Figure 7. (a–b) Nusselt number for lower and upper heated walls for various Grashof number.

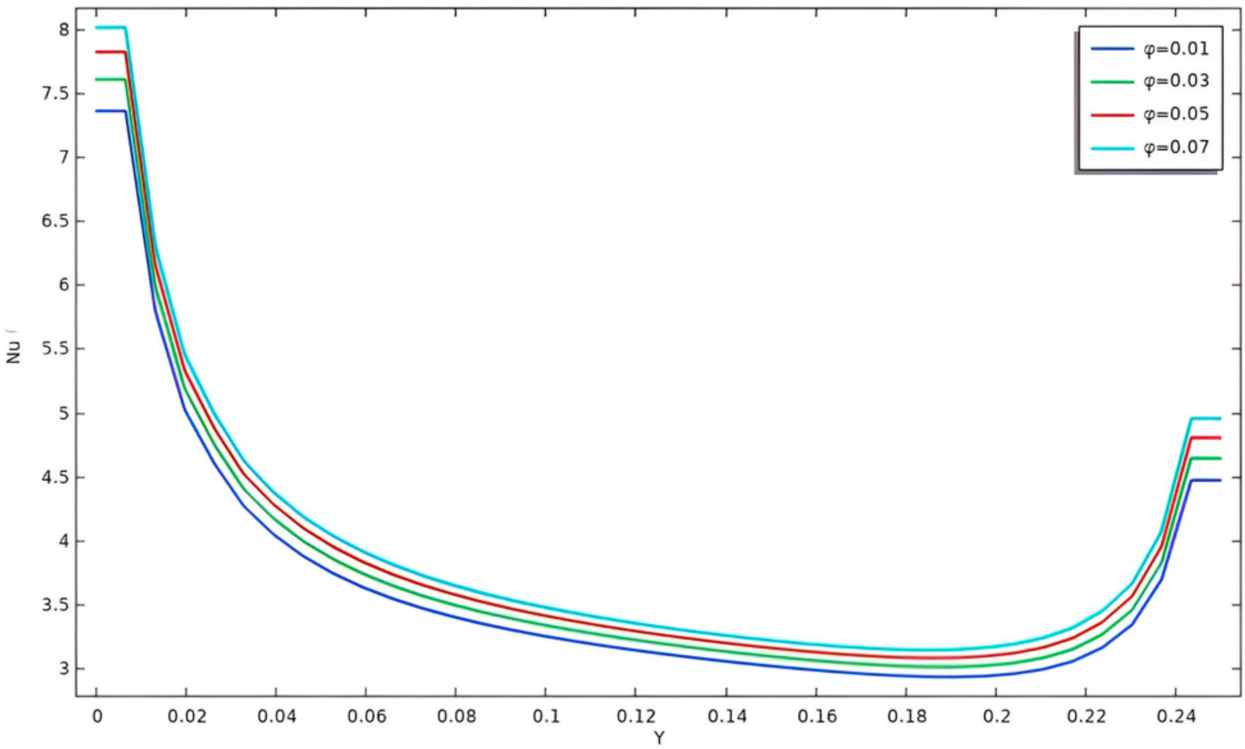

(a)

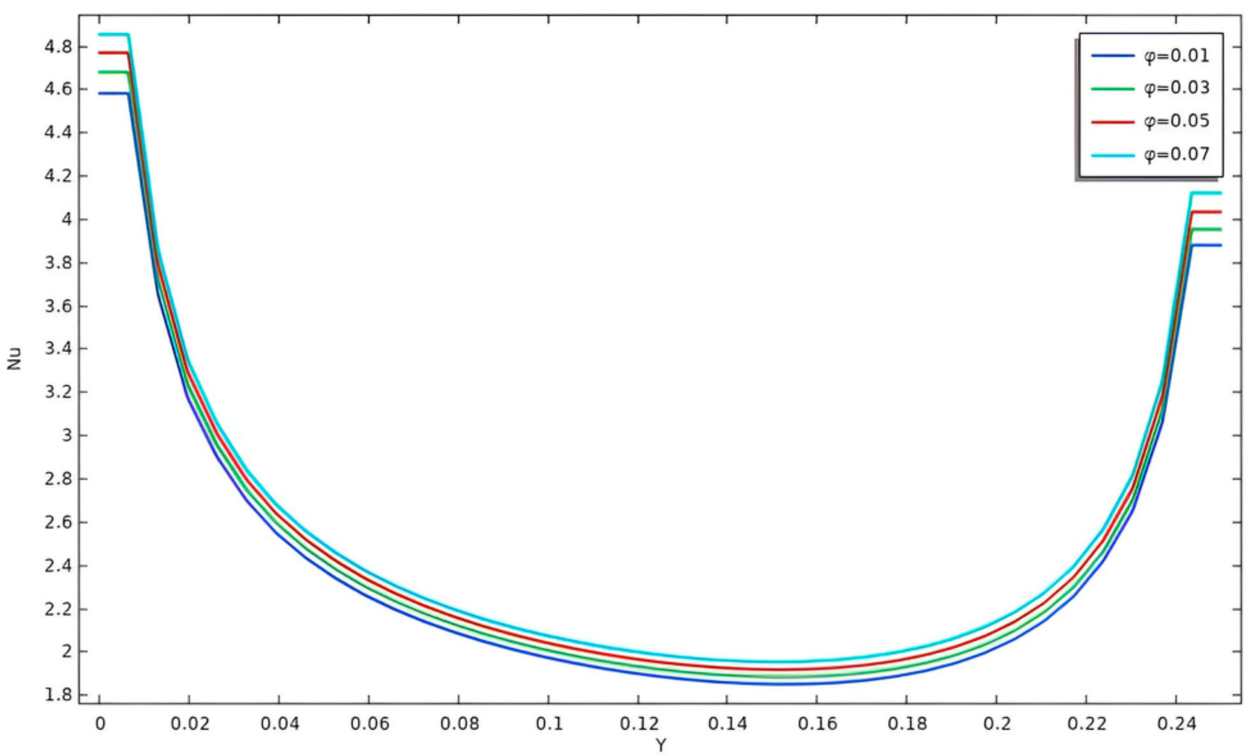

(b)

Figure 8. (a–b) Variation of Nusselt number on changing volume fraction of nanoparticles.

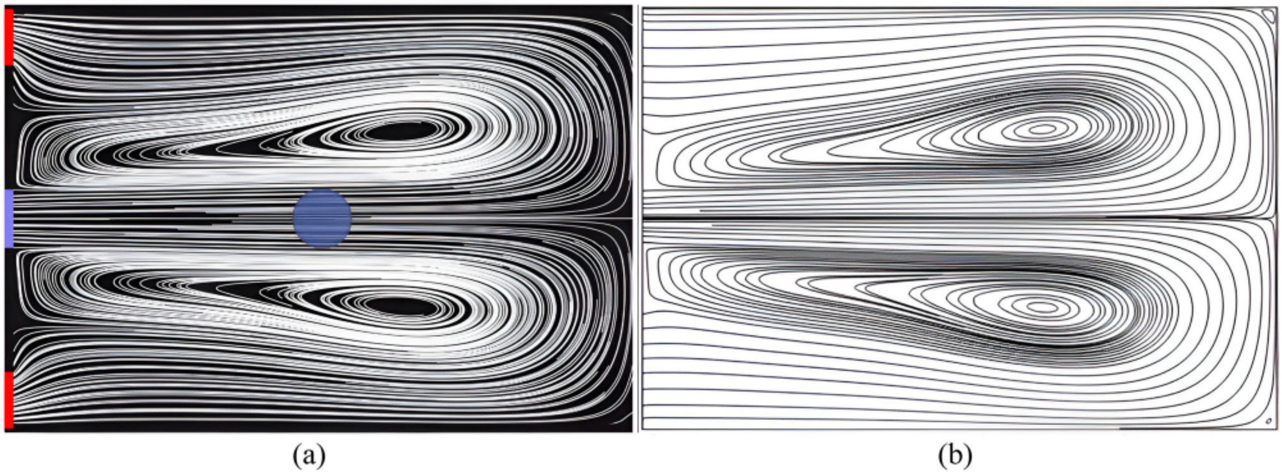

Figure 9. Comparative streamlines. (a) Williams et al. (2020). (b) Present results.

- Isotherm and streamline patterns show enhanced fluid mixing and convective heat transfer, providing insights for improving cooling and irrigation during ureteroscopy. Precise temperature regulation is crucial for tissue protection.
- The observed impacts of nanoparticle volume fractions on heat transfer efficiency provide guidelines for choosing nanofluids with suitable thermal characteristics. For example, the decrease in Nusselt number at greater nanoparticle concentrations aids in selecting the best formulations.
- Efficient heat evacuation from laser ablation sites is critical in ureteroscopy. The findings of this study, which include the impact of Reynolds and Grashof numbers on kinetic energy and heat dissipation, indicate design improvements for irrigation systems and reservoirs in surgical equipment.

Future research on nanofluid flow in a square cavity should focus on experimental validation to complement numerical studies, ensuring accurate real-world applicability. Further, specific modelling tailored to ureteroscopy to strengthen the connection between nanofluid dynamics and operational benefits in medical scenarios can also be the topic of interest. Additionally, incorporating hybrid nanoparticles can further enhance thermal properties and system performance.

Acknowledgements

All procedures were conducted in research that did not entail human or animal subjects or data.

Authors' contribution

All authors contributed equally have read and approved the final version of the manuscript.

Disclosure statement

No potential conflict of interest was reported by the author(s).

Use of Artificial Intelligence (AI) tools declaration

The authors declare that they have not used AI tools in the creation of this article.

Data availability statement

The data that support the findings of this study are available from the corresponding author upon reasonable request.

References

Ahmad, S., Cham, B. M., Liu, D., Islam, S. U., Hussien, M. A., & Waqas, H. (2024). Numerical analysis of heat and mass transfer of MHD natural convection flow in a cavity with effects of source and sink. *Case Studies in Thermal Engineering*, *53*, 103926. https://doi.org/10.1016/j.csite.2023.103926

Ahmad, S., Liu, D., Waqas, H., & Munir, S. (2024). Numerical simulation of magnetohydrodynamics double-diffusive natural convection in a cavity with non-uniform heated walls. *Applied Thermal Engineering*, *253*, 123778. https://doi.org/10.1016/j.applthermaleng.2024.123778

Ali, M. M., Akhter, R., & Alim, M. A. (2021). Performance of flow and heat transfer analysis of mixed convection in Casson fluid filled lid driven cavity including solid obstacle with magnetic impact. *SN Applied Sciences*, *3*(1), 1–15. https://doi.org/10.1007/s42452-020-03978-3

Amin, A., Munir, S., & Farooq, U. (2024). Flow dynamics and convective transport analysis of two-layered dissipative Casson hybrid nanofluid flow in a vertical channel. *Proceedings of the Institution of Mechanical Engineers, Part C: Journal of Mechanical Engineering Science*, *238*(2), 395–404. https://doi.org/10.1177/09544062231170753

Basak, T., Roy, S., Sharma, P. K., & Pop, I. (2009). Analysis of mixed convection flows within a square cavity with linearly heated side wall (s). *International Journal of Heat and Mass Transfer*, *52*(9-10), 2224–2242. https://doi.org/10.1016/j.ijheatmasstransfer.2008.10.033

Bilal, S., Khan, N. Z., Shah, I. A., Awrejcewicz, J., Akgül, A., & Riaz, M. B. (2021). Heat and flow control in cavity with cold circular cylinder placed in non-Newtonian fluid by performing finite element simulations. *Coatings*, *12*(1), 16. https://doi.org/10.3390/coatings12010016

Choi, S. U. (2009). Nanofluids: From vision to reality through research.

Dutta, S., Pati, S., & Baranyi, L. (2021). Numerical analysis of magnetohydrodynamic natural convection in a nanofluid filled quadrantal enclosure. *Case Studies in Thermal Engineering*, *28*, 101507. https://doi.org/10.1016/j.csite.2021.101507

Eid, A., Khader, M. M., & Megahed, A. M. (2022). Numerical treatments for the MHD flow of a viscous Newtonian fluid due to a porous shrinking sheet. *International Journal of Modern Physics C*, *33*(10), 2250136. https://doi.org/10.1142/S0129183122501364

Ganesan, K., Naresh Babu, M., Santhanakumar, M., & Muthukrishnan, N. (2018). Experimental investigation of copper nanofluid based minimum quantity lubrication in turning of H 11 steel. *Journal of the Brazilian Society of Mechanical Sciences and Engineering*, *40*(3), 1–17. https://doi.org/10.1007/s40430-018-1093-9

Gao, X. W., Liu, H., Cui, M., Yang, K., & Peng, H. (2019). Free element method and its application in CFD. *Engineering Computations*, *36*(8), 2747–2765. https://doi.org/10.1108/EC-10-2018-0471

Han, T., Zhang, C., & Luo, J. (2018). Macroscale superlubricity enabled by hydrated alkali metal ions. *Langmuir*, *34*(38), 11281–11291. https://doi.org/10.1021/acs.langmuir.8b01722

Ishii, H., Griffin, S., & Somani, B. K. (2015). Ureteroscopy for stone disease in the paediatric population: A systematic review. *BJU International*, *115*(6), 867–873. https://doi.org/10.1111/bju.12927

Kum, F., Mahmalji, W., Hale, J., Thomas, K., Bultitude, M., & Glass, J. (2016). Do stones still kill? An analysis of death from stone disease 1999–2013 in England and Wales. *BJU International*, *118*(1), 140–144. https://doi.org/10.1111/bju.13409

Li, D., & Li, H. (2024). Electromagnetohydrodynamic (EMHD) flow of Jeffrey fluid through parallel plate microchannels with surface charge-dependent asymmetric slip. *Physics Letters A*, *528*, 130026. https://doi.org/10.1016/j.physleta.2024.130026

Li, Z., Qing, J., Shen, C., Ma, S., Wu, D., Zhu, G., & Su, J. (2024). Study on performance optimization of double screw-magnetic fluid combination seal. *Physics of Fluids*, *36*(2), 022021. https://doi.org/10.1063/5.0190569

Lin, Y., Li, B., Zheng, L., & Chen, G. (2016). Particle shape and radiation effects on Marangoni boundary layer flow and heat transfer of copper-water nanofluid driven by an exponential temperature. *Powder Technology*, *301*, 379–386. https://doi.org/10.1016/j.powtec.2016.06.029

Lu, D. C., Farooq, U., Hayat, T., Rashidi, M. M., & Ramzan, M. (2018). Computational analysis of three layer fluid model including a nanomaterial layer. *International Journal of Heat and Mass Transfer*, *122*, 222–228. https://doi.org/10.1016/j.ijheatmasstransfer.2018.01.080

Mahdavi, M., Sharifpur, M., Ahmadi, M. H., & Meyer, J. P. (2020). Nanofluid flow and shear layers between two parallel plates: A simulation approach. *Engineering Applications of Computational Fluid Mechanics*, *14*(1), 1536–1545. https://doi.org/10.1080/19942060.2020.1844806

Malik, M. F., Turabi, Y. U. U. B., Raza, M., Imran, M., & Muhammad, T. (2024). Computational analysis of heat transfer for hybrid nanofluid flow within a wavy lid-driven cavity with entropy generation and non-uniform heating. *Results in Physics*, *67*, 108054. https://doi.org/10.1016/j.rinp.2024.108054

Moore, R. G., Bishoff, J. T., Loenig, S., & Docimo, S. G. (2005). *Minimally invasive urological surgery*. CRC Press.

Munir, S., & Amin, A. (2024). HAM-based analysis of nonlinear convection of two-layer water and air-TiO2 flow model in a vertical channel. *Numerical Heat Transfer, Part A: Applications*, *85*(9), 1517–1534. https://doi.org/10.1080/10407782.2023.2277826

Munir, S., & Turabi, Y. U. U. B. (2024). Impact of heated wavy wall and hybrid nanofluid on natural convection in a triangular enclosure with embedded cold cylinder under inclined magnetic field. *Arabian Journal for Science and Engineering*, *50*, 4007–4020.

Nguyen, V. T., & Sagar, H. J. (2024). Computational fluid dynamics modeling and experiments of two-phase flows. *Fluids*, *9*(9), 207. https://doi.org/10.3390/fluids9090207

Omar, M., Chaparala, H., Monga, M., & Sivalingam, S. (2015). Contemporary imaging practice patterns following ureteroscopy for stone disease. *Journal of Endourology*, *29*(10), 1122–1125. https://doi.org/10.1089/end.2015.0088

Rahman, M. M., Alim, M. A., Saha, S., & Chowdhury, M. K. (2009). Effect of the presence of a heat conducting horizontal square block on mixed convection inside a vented square cavity. *Nonlinear Analysis: Modelling and Control*, *14*(4), 531–548. https://doi.org/10.15388/NA.2009.14.4.14472

Sarmiento-Laurel, C., Cardemil, J. M., & Calderón-Muñoz, W. R. (2022). Local entropy generation model for numerical CFD analysis of fluid flows through porous media, under laminar and turbulent regimes. *Engineering Applications of Computational Fluid Mechanics*, *16*(1), 804–825. https://doi.org/10.1080/19942060.2022.2040595

Stamatelou, K. K., Francis, M. E., Jones, C. A., Nyberg, L. M., & Curhan, G. C. (2003). Time trends in reported prevalence of kidney stones in the United States: 1976–1994. *Kidney International*, *63*(5), 1817–1823. https://doi.org/10.1046/j.1523-1755.2003.00917.x

Sun, L., Wang, G., & Zhang, C. (2024). Experimental investigation of a novel high performance multi-walled carbon nano-polyvinylpyrrolidone/silicon-based shear thickening fluid damper. *Journal of Intelligent Material Systems and Structures*, *35*(6), 661–672. https://doi.org/10.1177/1045389X231222999

Turabi, Y. U. U. B., & Munir, S. (2024). CFD simulations of MHD effects on mixed convectional flow in a lid-driven square cavity with square cylinder using Casson fluid. *Numerical Heat Transfer, Part B: Fundamentals*, *86*(11), 1–16.

Wang, X. W., Wan, Z. P., & Tang, Y. (2013). Heat transfer mechanism of miniature loop heat pipe with water-copper nanofluid: Thermodynamics model and experimental study. *Heat and Mass Transfer*, *49*(7), 1001–1007. https://doi.org/10.1007/s00231-013-1144-9

White, F. M., & Majdalani, J. (2006). *Viscous fluid flow*. McGraw-Hill.

Williams, J. G., Castrejon-Pita, A. A., Turney, B. W., Farrell, P. E., Tavener, S. J., Moulton, D. E., & Waters, S. L. (2020). Cavity flow characteristics and applications to kidney stone removal. *Journal of Fluid Mechanics*, *902*, A16. https://doi.org/10.1017/jfm.2020.583

Wright, A. E., Rukin, N. J., & Somani, B. K. (2014). Ureteroscopy and stones: Current status and future expectations. *World Journal of Nephrology*, *3*(4), 243. https://doi.org/10.5527/wjn.v3.i4.243

Yan, S. R., Toghraie, D., Hekmatifar, M., Miansari, M., & Rostami, S. (2020). Molecular dynamics simulation of water-copper nanofluid flow in a three-dimensional nanochannel with different types of surface roughness geometry for energy economic management. *Journal of Molecular Liquids*, *311*, 113222. https://doi.org/10.1016/j.molliq.2020.113222

Zandie, M., Moghaddas, A., Kazemi, A., Ahmadi, M., Feshkache, H. N., Ahmadi, M. H., & Sharifpur, M. (2022). The impact of employing a magnetic field as well as Fe3O4 nanoparticles on the performance of phase change materials. *Engineering Applications of Computational Fluid Mechanics*, *16*(1), 196–214. https://doi.org/10.1080/19942060.2021.2006092

Zeng, W., Zhou, P., Wu, Y., Wu, D., & Xu, M. (2024). Multi-cavitation states diagnosis of the vortex pump using a combined DT-CWT-VMD and BO-LW-KNN based on motor current signals. *IEEE Sensors Journal*, *24*(19), 30690–30705. https://doi.org/10.1109/JSEN.2024.3446170

Zhang, G., Luo, J., Sun, M., Yu, Y., Wang, J., Chen, B., & Zhang, Z. (2025). Effect of soft magnetic particles content on multi-physics field of magnetorheological composite gel clutch with complex flow channel excited by Halbach array arrangement. *Composites Part A: Applied Science and Manufacturing*, *188*, 108576. https://doi.org/10.1016/j.compositesa.2024.108576

Zhou, L., Zhang, A., Ding, S., Han, S., Li, F., & Kujala, P. (2024). Numerical study of the cavitation performance of an ice-blocked propeller considering the free surface effect. *Water*, *16*(22), 3260. https://doi.org/10.3390/w16223260